SolarPACES 2024, 30th International Conference on Concentrating Solar Power, Thermal, and Chemical Energy Systems

Analysis and Simulation of CSP and Hybridized Systems

https://doi.org/10.52825/solarpaces.v3i.2459

Published: 22 Sep. 2025

Design Data for Alloy 282 High Temperature Concentrating Solar Power Components

SolarPACES

Bipul Barua[1,*], Mark C. Messner[1], and Michael D. McMurtrey[2]

[1]Argonne National Laboratory, USA

[2]Idaho National Laboratory, USA

*Correspondence: Bipul Barua, barua@nal.gov

Abstract. New design rules for high temperature concentrating solar power metallic components have been proposed recently. These rules are to be used in conjunction with the Section III, Division 5 rules of the ASME Boiler & Pressure Vessel Code and include three design by analysis options. In this paper, we report the corresponding design data for a nickel-based high temperature alloy – Alloy 282. The current Alloy 282 Code Case includes some basic material properties such as Young's modulus, Poisson's ratio, thermal properties, yield strength, tensile strength, and allowable stress S_o. However, a complete design check for high temperature components requires additional material data including allowable stress S_m, isochronous stress-strain curves, minimum-stress-to-rupture, fatigue diagrams, and creep-fatigue damage envelope. We construct these design data from the available material data in the literature and data generated recently at Idaho National Laboratory. We also develop an inelastic constitutive model for use with the design by inelastic analysis method.

Keywords: Solar Receiver, High Temperature Design, Creep, Creep-Fatigue

1. Introduction

To meet the Department of Energy's SunShot 2030 goal of reducing solar electricity costs by 50%, Concentrating Solar Power (CSP) towers must integrate with high-efficiency power cycles, such as closed-loop sCO2 Brayton cycles [1]. This integration requires raising the heat transfer fluid (HTF) outlet temperature of CSP receivers from 565°C in current systems to 720°C in next generation systems, resulting in peak receiver temperatures approaching 800°C [2]. At these elevated temperatures, creep and creep-fatigue failures become important design considerations for current metallic alloys, including high temperature superalloys like Alloy 282 [3].

The current ASME BPVC Section III, Division 5 [4] design rules for high-temperature components were originally developed for nuclear systems, which operate with long, stable periods. In contrast, CSP systems experience shorter diurnal cycles and frequent cloud transients. To address these conditions and the lower consequences of failure in CSP systems, Barua et al. [5] proposed new design rules for high-temperature CSP components, adapting the Section III, Division 5 rules to account for these differences. The proposed rules offer three design options:

- Option A: Elastic analysis with reduced margins.
- Option B: Elastic analysis with reduced margins and simplified creep-fatigue evaluation.
- Option C: Inelastic analysis using a simplified model.

Design options B and C apply only to alloys with high elevated temperature yield strength and include an additional requirement – the elastically calculated total stress intensity must be below the material's yield strength. Option C employs a simplified inelastic analysis based on a history-independent constitutive model describing the material's elastic-creep response. A detailed set of rules for each design option, along with their rationale, is provided in [5]. A brief summary of the rules is outlined below.

1.1 Design criteria

The proposed rules categorize the design checks for high-temperature CSP metallic components into four categories – (i) primary load checks, (ii) buckling criteria, (iii) ratcheting limits, and (iv) creep-fatigue criteria. The primary load checks and buckling criteria are consistent across all three design options.

The proposed primary load checks are essentially the same as the Section III, Division 5 primary load design limit checks, which involve comparing elastically calculated primary stress intensities to the time-independent allowable stress, S_o. However, the proposed rules exclude the primary load service limit checks from Section III, Division 5.

The proposed buckling criteria use Griffin's method of isochronous curves. A design passes if it avoids buckling when subjected to loads increased by a factor of 1.5 in an elastic-plastic analysis using temperature-dependent, isochronous stress-strain curves. Zero-time (hot tensile) curves are used for time-independent checks, while curves corresponding to the component's design life are used for time-dependent checks.

For ratcheting limit checks, Options A and B follow the B1 test from Section III, Division 5, HBB-T-1332 but with adjustments – (i) remove the 25% additional margin on core stress, σ_c for creep strain calculations, and (ii) increase allowable strains to 2% for base metal and 1% for welds. Option C uses elastic-creep analysis, with allowable strains of 10% for base metal and 5% for welds, doubling the Section III, Division 5 pointwise limits.

The proposed rules use the Section III, Division 5 approach for creep-fatigue criteria:

$$D_f + D_c \leq D \tag{1}$$

where $D_f = \Sigma \frac{N}{N_f}$ is the fatigue damage, $D_C = \Sigma \frac{t}{t_r}$ the creep damage, and D the total allowable damage provided by the creep-fatigue interaction diagram. Here, N is the number of load cycles at a fixed strain range and temperature, N_f the number of cycles to failure determined from fatigue diagrams, t the hold time at a fixed stress and temperature, and t_r the time-to-rupture determined from minimum stress-to-rupture/time/temperature relations. Option A adapts Section III, Division 5 design-by-elastic analysis method with a few adjustments – (i) use HBB-T-1413 for strain range calculations, (ii) use HBB-T-1433(a) for creep damage calculations, and (iii) use $1.0\sigma_c$ for stress relaxation instead of $1.5\sigma_c$, reflecting lower failure consequences for CSP. Option B further simplifies Option A by assuming high-strength materials like Alloy 282 will not yield in service, thus modifying the elastically calculated strain range only for creep deformation and using elastically calculated stresses for creep damage. Option C follows the design-by-inelastic analysis method of Section III, Division 5 but uses a simpler, elastic-creep model, thus omitting time-independent plastic deformation for the same reason as in Option B. The method also adjusts the factor *K'*, used to divide the stress history before calculating creep damage, from 0.67 to 0.9.

All options reduce fatigue design margins – the factors for strain range and cycles to failure are reduced from 2 and 20 to 1.5 and 10, respectively.

1.2 Require material design data

The proposed design methodology is based on a design by analysis approach which has two components – a method of analysis and design checks on the analysis results. Table 1 provides a list of the necessary material design data required for completing the design analysis and checks. Several commercial nickel-based alloys, including Alloy 625, Alloy 740H, Alloy 230, and Alloy 282, have been identified as potential materials for high-temperature CSP components [6].

This paper presents the material design data for Alloy 282 (UNS: N07208) as it pertains to the discussed design rules.

Table 1. *Required material properties and design data for high temperature CSP components.*

Analysis/design checks	*Required design data*
Thermal analysis	Thermal conductivity, thermal diffusivity, Coefficient of thermal expansion
Structural analysis	Elastic modulus, Poisson's ratio, Material constitutive model
Deign checks	Yield strength, Tensile strength, Allowable stress *So*, Allowable stress *Sm*, Minimum stress to rupture, Fatigue design charts, Creep-fatigue damage envelop, Isochronous stress-strain curves

2. Construction of design data

2.1 Physical properties, strengths and allowable stresses

Table 2 lists thermal conductivity; thermal diffusivity; mean and instantaneous coefficients of thermal expansion (CTE); and Young's modulus, *E*. These data come from Alloy 282 Code Case 3024 [7], except for instantaneous CTE, which was calculated from mean CTE. The Poisson's ratio is 0.31 [7].

Table 3 lists the tensile strength, S_u and yield strength, S_y. These data come from Alloy 282 Code Case 3024 [7] and listed in Table 2. The allowable stress, S_o is required for primary load design checks. This data comes from Alloy 282 Code Case 3024 [7] and listed in Table 2. Allowable stress, S_m is a temperature dependent, time-independent allowable stress and defined by the lesser of – (i) the specified minimum tensile strength divided by 3, (ii) the minimum specified yield strength multiplied by 0.67, (iii) the tensile strength at temperature divided 3, (iv) yield strength at temperature multiplied by 0.67. While this quantity is not directly used as an allowable stress in the proposed design rules, it is used in the ratcheting and creep-fatigue rules to determine the initial cyclic relaxation stress following the $3\bar{S}_m$ criterion. The calculated S_m values, based on S_y and S_u, are listed in Table 3.

2.2 Minimum-stress to rupture, S_r

The minimum stress-to-rupture (S_r) is the stress that will cause rupture in a specified time at a given temperature, representing a reasonable lower-bound material response. This is typically determined through a creep rupture test. However, it is impractical to conduct enough creep tests to cover all stress and temperature conditions needed for design calculations. Additionally, some designs would require tests lasting over 30 years, while most creep test data is for much shorter durations. Therefore, a predictive model, calibrated with creep rupture test data, is used to estimate design rupture stress. We applied the Larson-Miller method for this:

$$LMP = T\,(C + \log_{10} t_r) = \; a_o + a_1 \log_{10}\sigma + a_2(\log_{10}\sigma)^2 + a_3(\log_{10}\sigma)^3 \qquad (2)$$

where LMP is the Larson-Miller parameter, T the test temperature in K, σ the applied stress, t_r the rupture time, and C, a_1, and a_2 are constants. Figure 1(a) shows the Larson-Miller model fit to the creep rupture test data – extracted from [8], along with the 95% confidence prediction bounds. The 95% lower confidence bound model was used to generate the minimum stress-to-rupture data as tabulated in Table 3.

Table 2. *Physical properties, strengths, and allowable stresses. # indicates extrapolated value.*

Temp. (°C)	*Thermal cond. (W/m-K)*	*Thermal diff. (10^{-6} m^2/s)*	*Mean CTE (10^{-6} mm/mm-K)*	*Inst. CTE (10^{-6} mm/mm-K)*	*Elastic modulus (GPa)*	*S_y (MPa)*	*S_u (MPa)*	*S_o (MPa)*	*S_m (MPa)*
20~40	10.2	2.86	11.6	12.1	218	621	1069	305	356
100	11.5	3.09	12.3	12.9	214	571	1069	305	356
200	13.3	3.39	12.6	12.6	208	554	1069	305	356
300	14.8	3.65	12.9	14.0	202	547	1050	300	350
400	16.3	3.90	13.2	14.7	196	537	1031	294	344
500	17.8	4.17	13.5	15.4	189	528	1024	293	341
600	19.4	4.44	13.8	16.1	182	527	1004	287	335
700	20.9	4.68	14.3	19.7	172	527	936	146	312
800	21.9	4.81	15.0	21.2	161	497	776	45	259
900	22.2	4.80	16.0	26.5	148	445#	649#	15#	216#

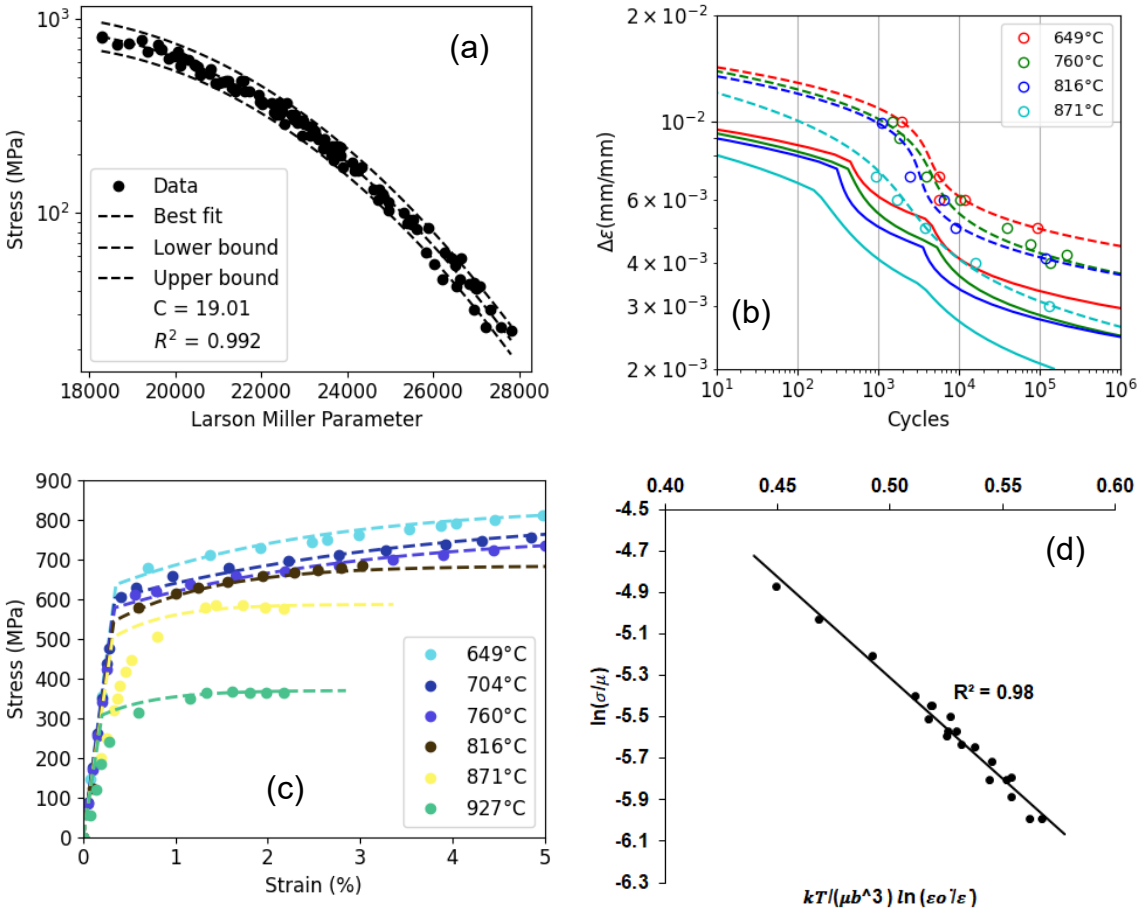

Figure 1. *(a) Larson-Miller model fit to creep rupture data; (b) fatigue data along with nominal (dashed lines) and design (solid lines) curves; (c) Voce hardening model fit to tensile data; and (d) Kocks-Mecking model fit to average creep rate to 2% creep strain data.*

Table 3. *Minimum stress to rupture.*

		Time (hours)									
		1	*10*	*30*	*100*	*300*	*1000*	*3000*	*10000*	*30000*	*100000*
Temperature (°C)	*425*	733	733	733	733	733	733	733	733	733	733
	500	733	733	733	733	733	731	723	708	689	663
	600	733	720	704	678	649	611	573	527	484	435
	700	668	588	543	490	441	386	338	287	245	202
	800	495	380	327	273	227	182	146	113	88	65
	900	296	193	153	116	88	63	46	31	22	14

2.3 Fatigue diagrams

Fatigue diagrams are typically derived from fully reversed, strain-controlled fatigue tests at a constant temperature. Figure 1(b) shows the fatigue test data from [9] along with the nominal fatigue curves fitted to the test data using:

$$N = 10^{\left(a_3(log_{10}\Delta\varepsilon)^3 + a_2(log_{10}\Delta\varepsilon)^2 + a_1(log_{10}\Delta\varepsilon) + a_0\right)} \tag{3}$$

where N is the number of cycles to failure, $\Delta\varepsilon$ the applied strain range, and a_0, a_1, a_2, and a_3 are constants. Figure 2(b) also shows the design fatigue curves, which include safety factors of 1.5 on the strain range and 10 on the cycles to failure.

2.4 Isochronous stress-strain relations

The proposed rules use isochronous stress-strain curves to represent creep deformation for evaluating ratcheting strain limits and assessing stress relaxation due to creep. These curves reflect the average stress required to achieve a specific total strain over time. Section III, Division 5 rules generate these curves by fitting a material model to available tensile and creep data, which we applied for Alloy 282 using tensile data from [8] and creep data from the literature [10]. The isochronous stress-strain model is based on an additive, history-independent breakdown of total strain (ε) into three components: elastic strain (ε_e), time-independent plastic strain (ε_p), and time-dependent creep strain (ε_c).

$$\varepsilon = \varepsilon_e + \varepsilon_p + \varepsilon_c \tag{4}$$

Hot tensile curves are a special case of this model when $\varepsilon_c = 0$, i.e., when time is zero. ε_e is calculated using the temperature dependent values of E.

$$\varepsilon_e = \frac{\sigma}{E} \tag{5}$$

ε_p is calculated using a Voce hardening model:

$$\varepsilon_p = \begin{cases} 0 & \sigma \le \sigma_1 \\ \frac{-1}{\delta}\ln\left(1 - \frac{\sigma-\sigma_1}{\sigma_p-\sigma_1}\right) & \sigma > \sigma_1 \end{cases} \tag{6}$$

where δ, σ_p, and σ_1 are model parameters which are calibrated using hot tensile curves. Figure 1(c) compares the hot tensile experiment with model curves. Table 4 lists the model parameters which should be be linearly interpolated between temperatures in the table. Finally, ϵ_c is calculated using the Kocks-Mecking [11,12] model.

$$\varepsilon_c = \dot{\varepsilon_o} e^{\frac{B\mu b^3}{AkT}} \left(\frac{\sigma}{\mu}\right)^{\frac{-\mu b^3}{AkT}} t \tag{7}$$

where $\mu = \frac{E}{2(1+\nu)}$ is the material share stress, *b* is the characteristic Burgers vector, k the Boltzman constant, $\dot{\varepsilon_o}$ the some reference strain rate, and *A* and *B* are model constants. Researchers [5,13,14] have successfully applied this method to model creep deformation and generate isochronous stress-strain curves for similar nickel-based alloys, Alloy 740H and Alloy 617, respectively. Figure 1(d) shows the model fit to Alloy 282 creep data [10], using the average rate to 2% creep strain as the deformation strain rate ($\dot{\varepsilon_c}$). Table 4 lists the model parameters. The choice of "average rate to 2% creep strain" for $\dot{\varepsilon_c}$ is based on the fact that Section III, Division 5 isochronous curves only provide data up to 2.2% total strain, which approximates 2% creep strain. The final design isochronous curves at a few temperatures are plotted in Figure 2 but Equations 4 to 7 and the parameters listed in Table 4 can be used to create the curves at any temperature between 649ºC and 927ºC.

Table 4. *Parameters for the ε_p and ε_c contribution to the isochronous stress-strain curves.*

T (°C)	*σ_1 (MPa)*	*σ_p (MPa)*	*δ*	*$\dot{\varepsilon_o}$ (hr^{-1})*	*b (mm)*	*A*	*B*
649	636.83	836.83	45.73	5.0×10^{8}	2.53×10^{-7}	-9.7316	-0.4444
704	602.57	817.57	30.26				
760	578.33	768.33	38.20				
816	544.19	684.19	96.68				
871	502.90	587.00	177.88				
927	307.78	370.00	176.54				

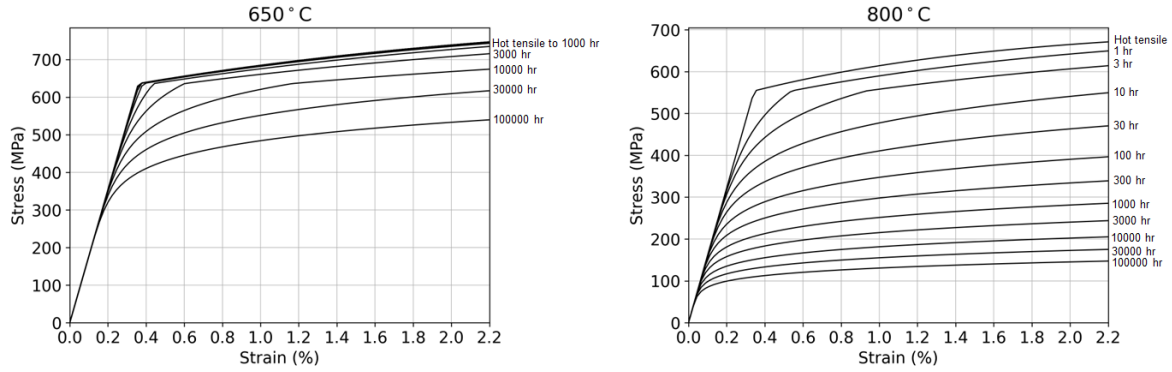

Figure 2. *Example isochronous stress-strain curves.*

2.5 Inelastic constitutive model

Design Option C in the proposed rules uses an elastic-creep analysis of the component, which can be executed with the following inelastic constitutive model:

$$\dot{\boldsymbol{\sigma}} = \boldsymbol{C}: (\dot{\boldsymbol{\varepsilon}} - \dot{\boldsymbol{\varepsilon}}_t - \dot{\boldsymbol{\varepsilon}}_c) \tag{8}$$

where $\dot{\boldsymbol{\sigma}}$ is the rate of the Cauchy stress tensor, $\boldsymbol{C}$ the isotropic elasticity tensor, $\dot{\boldsymbol{\varepsilon}}$ the total strain rate, $\dot{\boldsymbol{\varepsilon}}_t$ the thermal strain rate given by:

$$\dot{\boldsymbol{\varepsilon}}_t = \alpha \dot{T} \boldsymbol{I} \tag{9}$$

with α the instantaneous coefficient of thermal expansion, $\dot{T}$ the temperature rate, and $\boldsymbol{I}$ the identity tensor, and the creep strain rate, $\dot{\boldsymbol{\varepsilon}}_c$ is given by:

$$\dot{\boldsymbol{\varepsilon}}_c = \dot{\varepsilon_o} e^{\frac{B\mu b^3}{AkT}} \left(\frac{\sigma_v}{\mu}\right)^{\frac{-\mu b^3}{AkT}} \frac{\boldsymbol{s}}{\sigma_v} \tag{10}$$

where $\sigma_v = \sqrt{\frac{3}{2}\boldsymbol{s}:\boldsymbol{s}}$, and $\boldsymbol{s}$ is the deviatoric stress tensor. The parameters for Equation 10 are listed in Table 5.

2.6 Creep-fatigue damage envelope

The damage envelope in a creep-fatigue interaction diagram represents the criteria for creep-fatigue damage and is derived from creep-fatigue tests. The results are converted to fatigue and creep damage fractions. Figure 5 displays experimental data [15] collected at INL and the damage envelope, which is defined by the interaction point (0.1, 0.1).

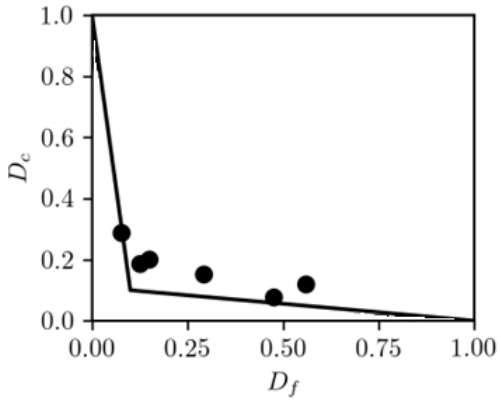

Figure 3. *Creep-fatigue damage envelope plotted on an interaction diagram along with the creep-fatigue test data.*

3. Conclusion

This paper provides design data for Alloy 282 to support high-temperature CSP component design using recently proposed rules adapted from ASME Section III, Division 5. The data include physical properties, allowable stresses, fatigue diagrams, minimum stress to rupture, creep-fatigue interaction diagram, isochronous stress-strain relations, and an inelastic constitutive model, enabling application of three design-by-analysis options:

Option A: Design by elastic analysis with reduced safety margins and modified creep-fatigue evaluation.

Option B: A simplified design by elastic analysis approach assuming no yielding.

Option C: Design by inelastic analysis based on a simplified elastic-creep model, assuming no yielding.

The design data should be adequate for designing Alloy 282 components for non-nuclear applications, though further testing may be needed to support weldments and address creep-fatigue failure.

Data availability statement

The material data used in receiver analysis is contained in the distribution of the *srlife* software, available at https://github.com/Argonne-National-Laboratory/srlife.

Underlying and related material

The underlying experimental data are available in ANL reports cited in the text.

Author contributions

Bipul Barua: Conceptualization, Formal analysis, Investigation, Methodology, Visualization, Data curation, Writing – original draft. **Mark C. Messner**: Conceptualization, Methodology, Funding acquisition, Writing – review & editing, Project administration, Resources. **Michael D. McMurtrey**: Investigation, Methodology, Data curation, Writing – review & editing.

Competing interests

The authors declare no competing interests.

Funding

This work was sponsored by the U.S. Department of Energy, under Contract No. DE-AC02-06CH11357 with Argonne National Laboratory, managed and operated by UChicago Argonne LLC. The authors gratefully acknowledge support from the U.S. Department of Energy through the Office of Energy Efficiency and Renewable Energy, Solar Energy Technologies Office, CSP Program.

Acknowledgement

Discussions with DOE project managers Dr. Kamala Raghavan and Dr. Vijaykumar Rajgopal are much appreciated.

References

[1] M. Mehos, et al. “Concentrating solar power Gen3 demonstration roadmap.” National Renewable Energy Laboratory technical report NREL/TP-5500-67464, 2017.
[2] Barua, B., M. C. Messner, and M. D. McMurtrey. "Comparison and assessment of the creep-fatigue and ratcheting design methods for a reference gen3 molten salt concentrated solar power receiver." Pressure Vessels and Piping Conference. Vol. 58943. American Society of Mechanical Engineers, 2019.
[3] B. Barua, and M. C. Messner. “Structural design challenges and implications for high temperature concentrating solar power receivers.” Solar Energy 251 (2023): 119-133.
[4] American Society of Mechanical Engineers Boiler & Pressure Vessel Code. Section III, Division 5.
[5] B. Barua, et al. “Design Guidance for High Temperature Concentrating Solar Power Components.” Argonne National Laboratory technical report ANL-20/03, 2020.
[6] Shingledecker, J., Purgert, R., & Rawls, P. (2014). Current status of the US DOE/OCDO A-USC materials technology research and development program. In 7th Int. Conf.: advances in materials technology for fossil power plants (pp. 41-52).
[7] American Society of Mechanical Engineers Boiler & Pressure Vessel Code. Code Case 3024 (approved on 07/22/2021).
[8] Alloy 282 Code Case data from ORNL, provided by DOE.
[9] http://haynesintl.com/docs/default-source/pdfs/new-alloy-brochures/high-temperature-alloys/brochures/282-brochure.pdf?sfvrsn=20
[10] Viswanathan, R. et al. Steam turnbine materials for ultrasupercritical coal power plants. DOE Award Number DE-FC26-05NT42442: Final Technical Report (2009).

[11] Kocks, U. F. (2001). Realistic constitutive relations for metal plasticity. Materials Science and Engineering: A, 317(1-2), 181-187.
[12] Estrin, Y., & Mecking, H. (1984). A unified phenomenological description of work hardening and creep based on one-parameter models. Acta metallurgica, 32(1), 57-70.
[13] Barua, B., et al. "Design Data for Alloy 740H High Temperature Concentrating Solar Power Components." Pressure Vessels and Piping Conference. Vol. 87486. American Society of Mechanical Engineers, 2023.
[14] Messner, M. C., & Sham, T. L. (2019, July). Isochronous stress-strain curves for Alloy 617. In Pressure Vessels and Piping Conference (Vol. 58929, p. V001T01A062). American Society of Mechanical Engineers.
[15] M.C. Messner, et al., “srlife: A Fast Tool for High Temperature Receiver Design and Analysis,” (No. ANL-22/29). Argonne National Lab.(ANL), Argonne, IL, 2022. (https://doi.org/10.2172/1871331).